JOURNAL OF AIRCRAFT
Vol. 38, No. 4, July–August 2001

Wake-Vortex Eddy-Dissipation Model Predictions Compared with Observations

T. Sarpkaya*
Naval Postgraduate School, Monterey, California 93943-5134
and
R. E. Robins† and D. P. Delisi‡
NorthWest Research Associates, Inc., Bellevue, Washington 98009-3027

The purpose of this paper is to describe the latest version of a wake-vortex eddy-dissipation model devised by T. Sarpkaya ("New Model for Vortex Decay in the Atmosphere," *Journal of Aircraft*, Vol. 37, No. 1, 2000, pp. 53–61.) and to compare its predictions with lidar observations obtained at Memphis and Dallas/Fort Worth airports. The model simulates the evolution of aircraft-generated trailing vortices in an atmospheric environment defined by vertical profiles of potential temperature, eddy-dissipation rate, and crosswind. Visual and quantitative comparisons of the time histories of altitude, circulation, and lateral position of predicted and measured vortices are presented.

Introduction

NASA[1,2] has undertaken to develop an Aircraft Vortex Spacing System (AVOSS), as an element of the Terminal Area Productivity program, to enhance the capacity of large airports by reducing wake-hazard-imposed aircraft separations for various flight modes and meteorological conditions. This, in turn, has required the development of heuristic vortex-evolution models, which can provide accurate real-time estimates of the length of time that a pair of trailing vortices will remain a hazard to any aircraft flying toward them. In what follows, sufficiently detailed descriptions of the latest version of the eddy-dissipation model devised by Sarpkaya[3] and the ground-effect algorithm devised by Robins et al.[4] are described, and comparisons of the model predictions with the field experiments[5–7] carried out at Memphis (MEM) and Dallas/Fort Worth (DFW) are presented.

Eddy-Dissipation Model

In this model the rate of change of impulse per unit length of the vortex wake is equated to the sum of the buoyancy force caused by stratification and the force caused by the rate of change of circulation. Thus, the model is similar to Greene's[8] approximate model of vortex decay in the atmosphere. However, there are two fundamental differences. The "drag force" in Greene's model is eliminated, and, more importantly, the nature of the rate of change of circulation is neither specified nor related to turbulence kinetic energy. The resulting equation is given in dimensional form by

$$2\pi\rho\frac{\mathrm{d}(Vb^2)}{\mathrm{d}t} = -\rho AN^2 z - \rho\frac{\mathrm{d}(b\Gamma)}{\mathrm{d}t} \tag{1}$$

where ρ is air density, V the wake descent speed, t the time, A the area of the wake oval, N the Brunt–Väisälä frequency, z the vertical elevation, Γ the vortex circulation, and b the vortex spacing (allowed to vary with time).

Sarpkaya[3] has previously hypothesized that the decay of the vortex pair is dictated by $\exp(-CT/T_c^*)$ where C is a constant, $T = V_0 t/b_0$, $V_0 = \Gamma_0/2\pi b_0$, b_0 is the initial vortex separation, T_c^* is the nondimensional time at which a catastrophic demise event (e.g., Crow instability,[9] core bursting) takes place, and Γ_0 is the initial vortex circulation, calculated from the reported aircraft type, weight, and speed. T_c^* is determined by ε^*, the normalized eddy-dissipation rate (EDR) as described next. Furthermore, it is assumed that the circulation of the vortex pair decays up to and beyond the said event. Formalizing this concept, we have

$$\frac{\Gamma}{\Gamma_0} = \exp\left[-\left(C + 0.25N^{*2}\right)\frac{T}{T_c^*(\varepsilon^*)}\right] \tag{2}$$

where N^* is the normalized stratification parameter ($=Nb_0/V_0$). Previously, Sarpkaya[3] used $C = 0.45$. A quantitative comparison of 219 out-of-ground-effect (OGE) MEM cases and 214 near-ground-effect (NGE) DFW cases, using the approach described by Robins and Delisi,[10] suggested $C = 0.55$. The term $0.25N^{*2}$ in the parentheses in Eq. (3) accounts for the effect of stratification on the enhancement of circulation decay. Model experiments have shown that its effect is negligible, except at very high stratifications. This is in conformity with full-scale experiments and large-eddy simulation.[3,5,6]

The justification for the proposed decay hypothesis rests with the experience gained from the analysis (Sarpkaya[11]) of the MEM and DFW field data, heuristic reasoning, and mathematical simplicity. It is hoped that a model having these features will also be robust and not overly sensitive to the uncertainties of the parameters specifying the atmospheric conditions, will apply equally well to all aircraft, stratification, and ambient turbulence, and will not require additional empirical constants. The model's dependence on the normalized eddy-dissipation rate [$\varepsilon^* = (\varepsilon b)^{1/3}/V_0$, where ε is the dimensional EDR] to include effects of ambient turbulence is regarded as particularly significant because ε^* is one of the most fundamental parameters of turbulence, particularly for flows capable of achieving a well-developed inertial subrange. The significance of the turbulence parameter ε^* was discussed by Crow and Bate[12] and has been used by Tombach[13] and Sarpkaya and Daly[14] in their work on trailing vortices.

The relationship between ε^* and T_c^* was first established by a model proposed by Crow and Bate.[12] Recently, Sarpkaya[11] removed some of the highly restrictive assumptions (to be noted later) in their analysis to arrive at a modified Crow–Bate model. Figure 1 shows the results from these models, in addition to experimental data,[14] and the results (lifetimes to linking) of the large eddy simulations by

Presented as Paper 2000-0625 at the 38th Aerospace Sciences Meeting and Exhibit, Reno, NV, 10–13 January 2000, received 18 April 2000; revision received 22 November 2000; accepted for publication 26 November 2000.

*Distinguished Professor of Mechanical Engineering, 700 Dyer Road. Associate Fellow AIAA.
†Research Scientist, P.O. Box 3027. Senior Member AIAA.
‡Senior Research Scientist & President, P.O. Box 3027. Senior Member AIAA.

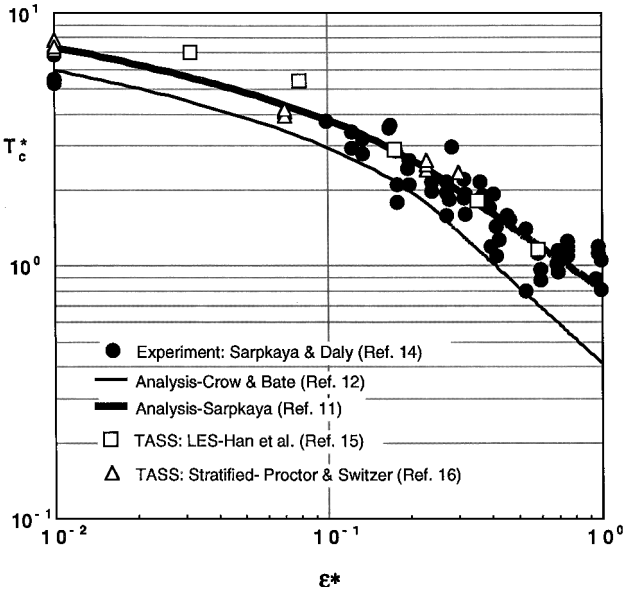

Fig. 1 T_c^* vs ε^*: models and physical and numerical experiments.

Han et al.[15] for a nonstratified medium and by Proctor and Switzer[16] for a stratified medium. In more complex environments the indirect effects of N^* on T_c^* also need to be taken into account.[17] Moreover, there are a number of issues regarding the variation of EDR and the indirect effects of stable and unstable stratification on the inception of one or more catastrophic demise events that require additional refinements in the proposed model.

Various turbulence regimes in Fig. 1 can be described as follows. In weak turbulence (i.e., for ε^* less than about 0.02 or for ε less than about 0.03 cm^2/s^3 for a DC-10 with $\Gamma = 550$ m^2/s and $b = 37$ m), multiple linking (with an average wavelength of about $7.8b$) and the subsequent instability events destroy the linear coherence of vortices. In medium turbulence (i.e., for ε^* greater than about 0.02 and less than about 0.2, a value equivalent to ε of about 30 cm^2/s^3 for the preceding DC-10) the dominant form of instability is the Crow instability (with decreasing wave lengths and integral length scales) and occasional vortex bursting. The physics of the latter is not understood, but it is known that bursts do not lead to reconnection. Finally, for stronger turbulence (i.e., for ε^* larger than about 0.2), vortex bursting, all other forms of instability, strong mixing in the overlapping region of the vortices, rollup of vortices about each other, and lateral displacements, spread the vorticity irreversibly over a large area.[13,14,17]

Figure 1 shows that the original Crow and Bate[12] model serves as a lower bound to the link/burst data. It becomes inadequate for $\varepsilon^* > 0.2$ where the predicted decay is quite steep. The reasons lie in the highly restrictive nature of some of the assumptions made in their pioneering analysis. The most important ones are as follows: 1) "The atmospheric turbulence is regarded as independent of the vortices."[12] In other words, the modification of the ambient turbulence by the trailing vortices and departures from statistical homogeneity and isotropy are not taken into account. 2) "The lifespan is determined by extrapolating linear theory to times when the displacement perturbations are comparable to the original vortex separations b."[12] 3) "The atmospheric turbulence is assumed to be steady in coordinates moving downward with the vortices."[12] As just noted, both the wavelength and the integral length scale decrease with increasing ε^*, at least in small-scale experiments. Crow and Bate[12] drew attention to the fact that "There seems to be no straightforward way to handle such departures, and the assumption that they are unimportant will have to be tested by comparing the calculated lifespans to experiment." It is in response to the comments of Crow and Bate[12] that their model was rederived,[11] as just noted, to allow for the variation of the wavelength and the integral length scale. The resulting vortex lifespans $T_c^* = T_c^*(\varepsilon^*)$ in various intervals, shown in Fig. 1, are represented by

for $T_c^* < 2.25$ or for $\varepsilon^* > 0.2535$

$$\varepsilon^* T_c^{*\frac{4}{3}} = 0.7475 \tag{3a}$$

for $2.25 < T_c^* < 7$ or for $0.0121 < \varepsilon^* < 0.2535$

$$\varepsilon^* = T_c^{*\frac{1}{4}} \exp\left(-0.7 T_c^*\right) \tag{3b}$$

for $7 < T_c^* < 9$ or for $0.001 < \varepsilon^* < 0.0121$

$$T_c^* = -180\varepsilon^* + 9.18 \tag{3c}$$

for $\varepsilon^* < 0.001$,

$$T_c^* = 9 \tag{3d}$$

Comparison of model predictions with the available field data has shown that results from the proposed model [Eqs. (2) and (3)] agree reasonably well with the available data in regions OGE. However, in some cases, usually for higher levels of ambient turbulence, the observed descents are faster than the calculated descents even though the predicted circulations agree with the measurements. This behavior can be modeled by using a slowly decreasing effective vortex separation, which, for a first order of approximation, accounts for the antisymmetric sinusoidal perturbation of the vortex pair (Crow instability) and its attendant consequences such as the decay of circulation with radius and the three-dimensional nature of the evolving vortices. In the present model the effective vortex spacing in the precatastrophic demise period ($T < T_c^*$) is represented by

$$\frac{b}{b_0} = \frac{(1+\alpha\varepsilon^*)}{(1-\alpha\varepsilon^*)} \frac{\left(1-\alpha\varepsilon^* e^{T/T_c^*}\right)}{\left(1+\alpha\varepsilon^* e^{T/T_c^*}\right)} \tag{4a}$$

Equation (4a) introduces a relatively mild variation in b/b_0. The constant α is taken to be 0.5 on the basis of comparisons with observations. Clearly, $b = b_0 = 1$ for $T = 0$. As T increases, the effect of the ambient turbulence enters into b/b_0 both directly, albeit nonlinearly, through $\alpha\varepsilon^*$ and, indirectly, through the exponent. This formulation was inspired by the work of Crow and Murman[18] and Sarpkaya,[17] who expressed a perturbation growth parameter in terms of the difference between the maximum and minimum vortex separation divided by their sum.

For $T > T_c^*$, vortex rings may form, or other strong deformations may occur. In other words, the descending vorticity may no longer be organized in parallel or nearly parallel coherent tubes. In such situations the concept of vortex separation becomes more complex, and one must construct an expression for b/b_0 that corresponds to $\Gamma/2\pi V$, where Γ is the circulation and V is the descent speed. In addition, this expression must match expression (4a) at $T = T_c^*$. Relying on physical intuition derived from previous work with complex vorticity distributions, we arrive at the following expression for $T > T_c^*$:

$$\frac{b}{b_0} = \frac{b\left(T_c^*\right)}{b_0} \times \left\{1 - \frac{2\alpha\varepsilon^* e/K}{1-(e\alpha\varepsilon^*)^2}\left[1 - \exp\left(-K\frac{T-T_c^*}{T_c^*}\right)\right]\right\} \tag{4b}$$

where $K = 5/\varepsilon^*$ and $\alpha = 0.5$.

Ground-Effect Algorithm

The complex problems posed by ground effect have been studied by a number of investigators. For low Reynolds numbers Zheng and Ash[19] have modeled the wake vortices near ground using an unsteady, two-dimensional laminar flow. For full-scale Reynolds numbers Burnham[20] presented numerous observations of the time history of trajectory, circulation, and core structure for vortices interacting with the ground. In many of these cases, the vortices were seen to rebound after their interaction with the ground. Kantha[21] proposed an "empirical model of transport and decay of wake vortices between parallel runways" using inviscid vortices primarily in ground effect. In fact, in a follow-up paper Kantha[22] noted that his

previous model[21] "assumed that the circulation around each vortex remains unchanged from its initial value of birth" and introduced six empirical constants to simulate decay. Puel and de Saint Victor[23] presented a calculation code, which solves the Navier–Stokes equations expressed in both unsteady two-dimensional form and steady three-dimensional form. They were able to reproduce the well-known theoretical solution of Lamb and Oseen, the rebound phenomenon, and the creation of secondary vortices. They have concluded that "the use of turbulence models must be considered to be able to deal with all these effects." Puel and de Saint Victor[23] have also noted in connection with Kantha's work[21] that "this type of model is still far from being able to predict correctly the evolution of the wake, it can only give a first outline at present."

Robins et al.[4] devised a ground-effect algorithm to augment Greene's model by extending earlier models (see, e.g., Corjon et al.[24]). This algorithm is also used to augment the current eddy-dissipation model. A summary of this algorithm is as follows: when the vortices approach an altitude of about $1.5b_0$ from the ground, a pair of inviscid image vortices are introduced, and the decay rate is assumed to remain identical to that existing just above $1.5b_0$. As the altitude of the vortices decreases further and reaches a level of $0.6b_0$, two new vortices (ground-effect vortices or secondary satellite vortices of relatively small strength) and their images are introduced, bringing the total number of real and image vortices to eight. Finally, when the satellite vortices have rotated 180 deg around the primary vortices, a second set of ground-effect vortices (and their images) is introduced, bringing the total number of vortices to 12. As in the image vortex region, the primary vortices (and their images) continue to decay in the ground-effect region at the rate that occurred just before the vortices entered the image vortex region. The main benefit of the ground-effect vortices is that they enable simulation of the rebound of the primary vortices, which is frequently observed.[20]

Comparison of Model Predictions to Observations

In this section we show some examples of how eddy-dissipation model (henceforth referred to as "model") predictions compare to observations. The OGE cases cited herein come from the 1995 MEM deployment and the NGE cases from the 1997 deployment at DFW. Both of these deployments were conducted by the AVOSS team at NASA's Langley Research Center. They included lidar measurements by the air traffic meteorology group of the Lincoln Laboratory at the Massachusetts Institute of Technology (MIT/LL). The efforts of the MIT team are described by Campbell et al.[5,6] and Dasey et al.[7]

Figures 2a–2d show a comparison of the data with the model predictions for the flight MEM1282, which occurred at the Memphis Armory site. At the top of the figure is the case identifier (MEM1282), the date and universal time of the case, and the generating aircraft. As noted on all plots, the circles and *x*s represent MIT/LL Lidar observations of the port and starboard vortices, respectively. Figure 2a shows a comparison of the predicted and measured positions of the vortices vs time. The two horizontal solid lines (identified on all figures as corridor floors) denote the upper and lower floors of a safety corridor, defined by Hinton,[1] for use by AVOSS. For a typical application of AVOSS, vortices remaining above the upper floor are a potential hazard for following aircraft. In Fig. 2a the vortices drop and stay below the upper floor after a time of approximately 70 s.

Figure 2b shows the circulation vs time (the initial circulation is given by $\Gamma_0 = W/\rho U b_0$, where W is aircraft weight, ρ is air density $= 1.2\ \mathrm{kg/m^3}$, and U is the aircraft speed). The data represent the averages from 3 to 10 m of the circulation, measured at radius intervals of 1 m.

Figure 2c shows the plan view of the predicted and observed altitudes of the vortices vs their lateral position. The meaning of the other lines are directly noted on the figure. For further clarification the topmost horizontal line marks the altitude of the glide slope, and the lower lines denote the upper and lower corridor floors. The side boundaries of the AVOSS corridor are off the plot. The vertical dotted line is midway between the initial lateral positions of the vortices and is used as the origin for plots of environmental profiles: a long dashed line for potential temperature, a solid line for cross wind, and a dot-dash line for EDR. Five meters in the lateral position represents 1 K of potential temperature, one meter per second

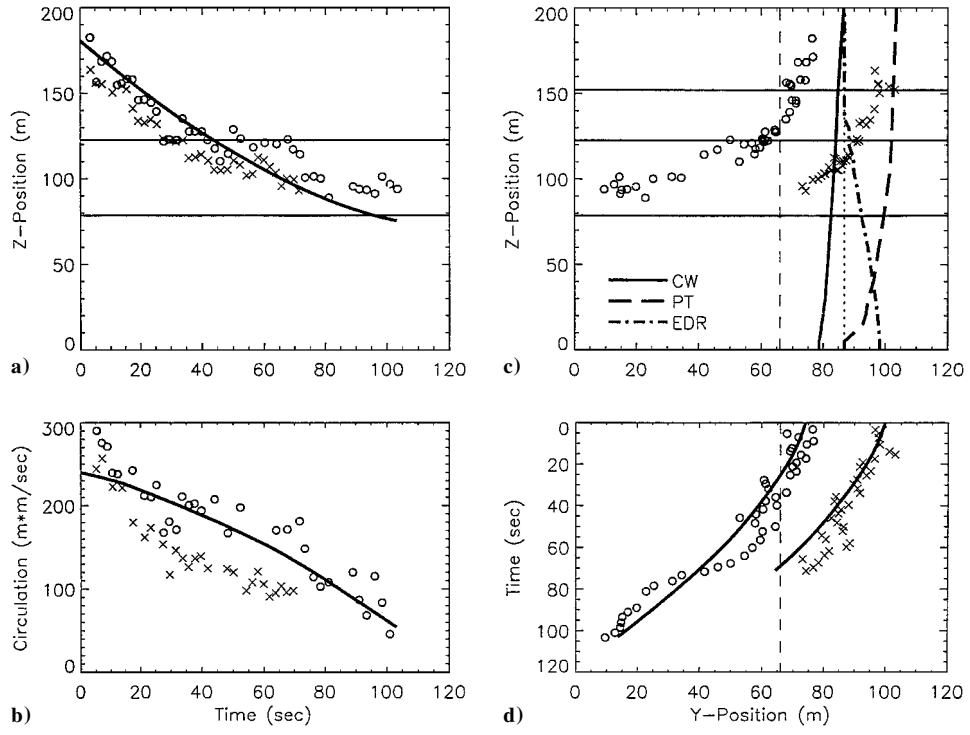

Fig. 2 Comparisons of model predictions with lidar observations for MEM case 1282. Observations are denoted by ∘ (port vortex) and × (starboard vortex), and in a), b), and d) model predictions are indicated by —— (model predictions are omitted from c) for simplicity). Horizontal —— in a) and c) define vertical AVOSS corridor boundaries. Environmental profiles appear in c), where 5 m in lateral position represents 1 m/s of crosswind (CW), 1 deg K of potential temperature (PT), and a unit value of log(EDR). The vertical . . . . . in c) denotes CW = 0, PT at the ground, and a value of − 6 for log(EDR). The vertical – – – in c) and d) indicates the runway centerline.

Table 1 Statistics for normalized differences between the predictions and observations

	rms $\Delta\Gamma/\Gamma_0$		rms $\Delta z/b_0$		rms $\Delta y/b_0$	
Airport (N)	Median	90th percentile	Median	90th percentile	Median	90th percentile
MEM (219)	0.15	0.28	0.42	0.93	0.76	2.27
DFW (214)	0.15	0.25	0.24	0.50	0.58	1.76

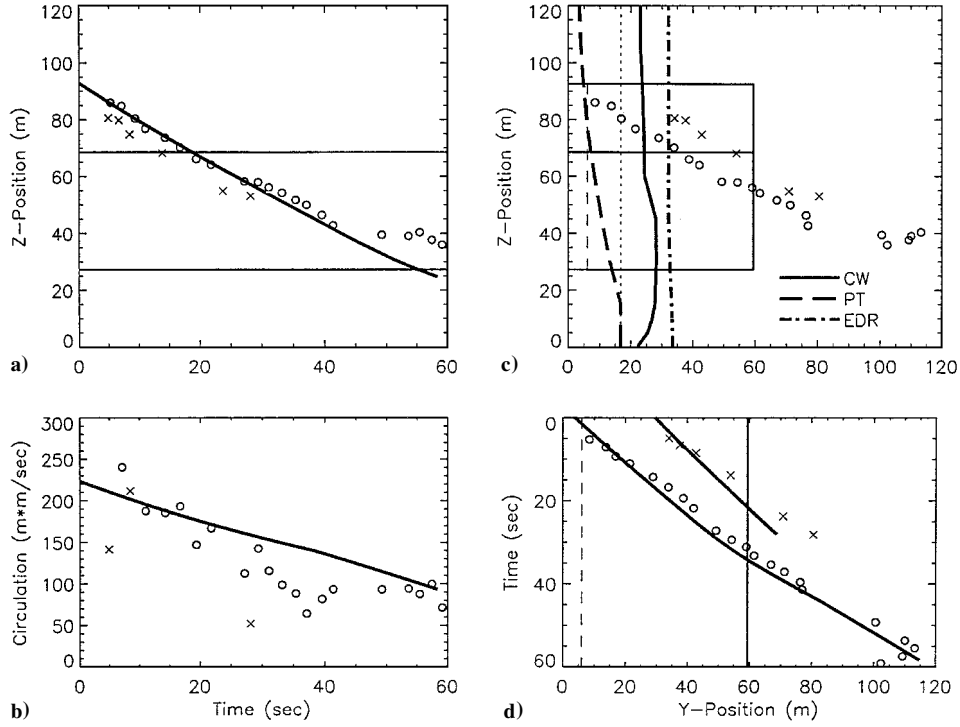

Fig. 3 Comparisons of model predictions with lidar observations for DFW case 970930_202905. Observations are denoted by ∘ (port vortex) and × (starboard vortex), and in a), b), and d) model predictions are indicated by —— (model predictions are omitted from c) for simplicity). Horizontal —— in a) and c) define AVOSS corridor boundaries, as do vertical —— in c) and d). Environmental profiles appear in c), where 5 m in lateral position represents 1 m/s of crosswind (CW), 1 deg K of potential temperature (PT), and a unit value of log(EDR). The vertical . . . . in c) denotes CW = 0, PT at the ground, and a value of − 6 for log(EDR). The vertical – – – in c) and d) indicates the runway centerline.

of crosswind, and one decade of EDR. Here we have plotted the base ten logarithm of EDR, with the dotted vertical line denoting a logarithm of -6 (EDR $= 10^{-6}$ m^2/sec^3). The dotted line also denotes the potential temperature at the ground and a zero crosswind.

For this case the potential temperature profile tells us that the atmosphere is statically stable near the ground and approaches neutral stability as altitude increases. It is seen that the crosswind is nearly 2 m/s toward port side at the ground level and gradually decreases to zero at an altitude of 200 m. EDR is between 10^{-4} and 10^{-3} at the ground and falls off to 10^{-6} at an altitude of about 135 m. Potential temperature and crosswind profiles are generated by MIT/LL from atmospheric measurements at several altitudes, and EDR profiles are estimated from observations at 5 and 40 m using an algorithm devised by the atmospheric boundary layer group at North Carolina State University.[25]

Figure 2d shows the lateral motion of the vortices as a function of time (note that time increases from the top to the bottom of the vertical axis). In this case the aircraft was about 20 m to the right of the runway centerline when it passed by the lidar, which was located just over 2500 m from the runway threshold.

Figures 3a–3d show a comparison of the data with the model predictions for the flight DFW970930-202905, which occurred at DFW runway 17C. The figure elements are the same as for Fig. 2, except that the title at the top of the figure omits date and time because these are included in the case identifier. One of the AVOSS corridor side boundaries appears as a vertical solid line in both Figs. 3c and 3d. The sign of the potential temperature profile in Fig. 3c corresponds to an unstable atmosphere, except near the ground where it is neutrally stable. The crosswind varies from 1 to nearly 3 m/s, toward starboard, reaching a peak at an altitude of 45 m. EDR varies from between 10^{-3} and 10^{-2} at the ground to about 10^{-3} at 120 m altitude.

The sample comparisons shown in Figs. 2 and 3, as well as many others (not shown here) from MEM and DFW, are quite encouraging. For a more comprehensive and quantitative comparison the approach outlined in Robins and Delisi[10] was applied to 219 OGE MEM cases and 214 NGE DFW cases. The results are presented in Table 1, the first column of which is denoted "Airport (N)," where Airport is either MEM or DFW, and N is the number of cases.

For each of the 219 MEM cases and 214 DFW cases, both predictions and observations were interpolated onto the same time grid. The square of the difference between the predicted and observed values for each case was then averaged over the duration of the measurements. The distribution of the square roots of these averages (the rms values) was then analyzed, and the median and 90th percentile rms values entered into the table. For a given case only the rms value for the vortex (port or starboard) with the most circulation observations was used.

It is evident from the table that the median and 90th percentile values for rms $\Delta z/b_0$ and rms $\Delta y/b_0$ are significantly smaller for DFW than for MEM. This disparity arises primarily because the durations for the MEM cases are generally longer than for the DFW cases, with the result that the predictions have more time to deviate

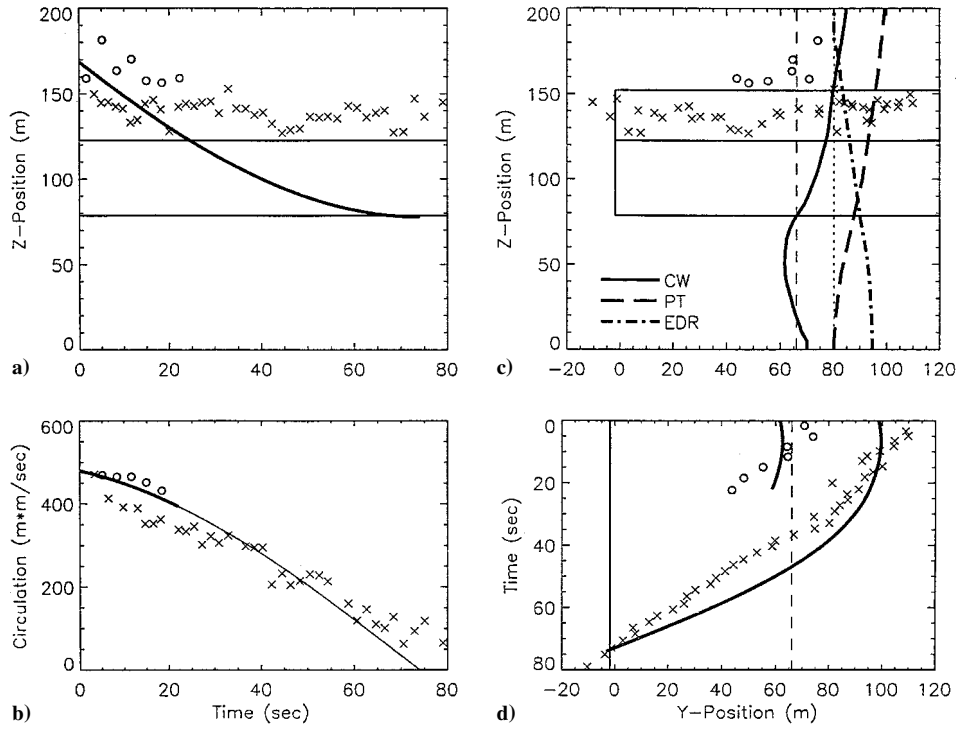

Fig. 4 Comparisons of model predictions with lidar observations for MEM case 1137. Observations are denoted by ∘ (port vortex) and × (starboard vortex), and in a), b), and d) model predictions are indicated by —— (model predictions are omitted from c) for simplicity). In b) the thicker (thinner) —— denotes the prediction for the (starboard) vortex. Horizontal —— in a) and c) define AVOSS corridor boundaries, as do vertical —— in c) and d). Environmental profiles appear in c), where 5 m in lateral position represents 1 m/s of crosswind (CW), 1 deg K of potential temperature (PT), and a unit value of log(EDR). The vertical . . . . in c) denotes CW = 0, PT at the ground, and a value of − 6 for log(EDR). The vertical – – – in c) and d) indicates the runway centerline.

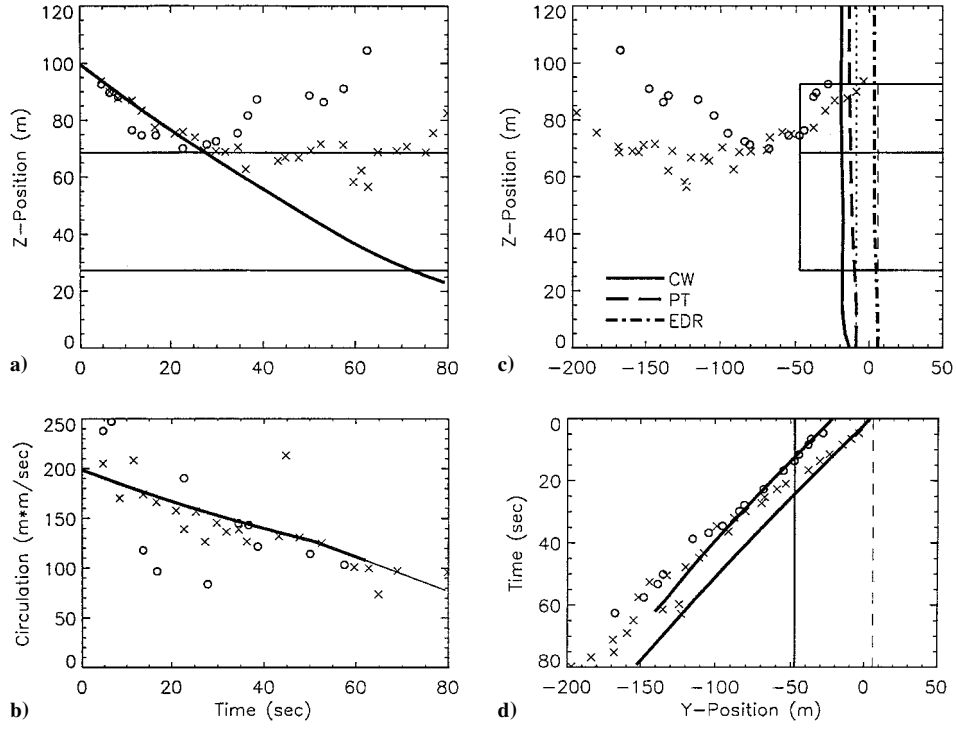

Fig. 5 Comparisons of model predictions with lidar observations for DFW case 970930_162314. Observations are denoted by ∘ (port vortex) and × (starboard vortex), and in a), b), and d) model predictions are indicated by —— (model predictions are omitted from c) for simplicity). In b) the thicker (thinner) —— denotes the prediction for the port (starboard) vortex. Horizontal —— in a) and c) define AVOSS corridor boundaries, as do vertical —— in c) and d). Environmental profiles appear in c), where 5 m in lateral position represents 1 m/s of crosswind (CW), 1 deg K of potential temperature (PT), and a unit value of log(EDR). The vertical . . . . in c) denotes CW = 0, PT at the ground, and a value of − 6 for log(EDR). The vertical – – – in c) and d) indicates the runway centerline.

from observations for MEM than for DFW. To quantify this duration difference, it is noted that the measurement times for the MEM cases varied from 16.9 to 163.7 s, with a median value of 58.0 s, whereas for the DFW cases the duration range was 13.5 to 146.0 s, and the median value was 43.2 s. One reason why MEM cases lasted longer than DFW cases was that ambient turbulence levels were generally higher for the DFW cases. Two explanations for this higher turbulence are: 1) the DFW cases were observed during the day whereas most of the MEM cases were observed during the evening, and 2) the starting altitudes for the DFW cases (73.5–130.3 m, median 96.4 m) were closer to the ground than for MEM (132.1–252.4 m, median 177.9 m). (We presume here, and observations confirm, that turbulence levels are higher for day than for evening and increase as altitude decreases.) Furthermore, crosswind speeds were generally higher for the DFW cases, with the result that DFW vortices were more often blown out of lidar range than MEM vortices.

It is also evident from Table 1 that the median and 90th percentile values for rms $\Delta y/b_0$ are greater than for rms $\Delta z/b_0$. This discrepancy arises because the observed crosswind profiles are not always representative of the actual crosswind at the location where the vortices are evolving. At both MEM and DFW winds were measured at least a mile from where the vortices were generated, and wind data were averaged so that temporal variations were not well represented.

For the model under discussion to be a useful tool for AVOSS, it is important to understand what is happening in the cases where the rms values are above the 90th percentile levels. For 16 of the 21 MEM and 10 of the 21 DFW cases for which RMS $\Delta z/b_0$ falls in the 90th percentile, the large deviations from observations were caused either by bad data (five DFW cases) or to the observed descent being more rapid than the predicted descent. In five of the MEM and 11 of the DFW cases, the large deviations were caused by the vortices descending less rapidly than predicted. An example of a MEM case for which the observed descent is slower than the prediction is shown in Fig. 4. Here the rms value of $\Delta z/b_0$ is 1.055, which is greater than the 90th percentile value of 0.93. Figure 5 shows a DFW case involving retarded descent for which the rms value of $\Delta z/b_0$ is 0.931, which is much greater than the 90th percentile value of 0.50. The agreement between the predicted and observed lateral positions and circulations in Figs. 4 and 5 is reasonably good, even though the agreement for altitude is not (see Figs. 4a and 5a). The thin solid line in Figs. 4b and 5b represents the circulation of the starboard vortex.

There are more retarded descent cases for DFW than MEM. This may be caused by the fact that more DFW cases occurred during daytime when convective activity, a possible cause of retarded descent, is more likely to occur. Efforts are currently underway to better understand when retarded descent cases may be expected. Such an understanding is important to AVOSS because under conditions favoring retarded descent AVOSS may have to exclude corridor clearance as a result of vertical transport as one of the criteria enabling reduced spacing of landing aircraft.

Summary

A newer version of the wake-vortex eddy-dissipation model devised by Sarpkaya[3] has been presented. The new features include a choice of 0.55 for the model constant C, allowance for time-varying vortex separation caused by three-dimensional effects, and a representation for the influence of stratification on circulation decay. A determination of the median and 90th percentile values for normalized rms differences between predictions and observations for over 400 cases (219 OGE cases from MEM and 214 NGE cases from DFW) have shown that the new model performs reasonably well. Further work is required to ascertain the atmospheric conditions under which model predictions are likely to significantly vary from observations.

Postscript: During the week of 17 July 2000 at DFW International Airport, the AVOSS team from NASA's Langley Research Center, led by D. A. Hinton, conducted a real-time demonstration of the airport capacity enhancement system they have been developing. The EDR algorithm described in this paper was used to generate the predictions of vortex evolution that are used by AVOSS to help determine when standard aircraft spacing distances can be safely reduced. The algorithm performed, in real time, without problems and routinely provided vortex evolution predictions that agreed favorably with real-time lidar observations.

Acknowledgments

We gratefully acknowledge the support and encouragement of D. A. Hinton and F. H. Proctor of NASA's Langley Research Center.

References

[1]Hinton, D. A., "An Aircraft Vortex Spacing System (AVOSS) for Dynamical Wake Vortex Spacing Criteria," NATO-AGARD-CP-584, 1996, pp. 5.1–5.9.

[2]Proctor, F. H., "Numerical Simulation of Wake Vortices Measured During Idaho Falls and Memphis Field Programs," AIAA Paper 96-2496, Jan. 1996.

[3]Sarpkaya, T., "New Model for Vortex Decay in the Atmosphere," *Journal of Aircraft*, Vol. 37, No. 1, 2000, pp. 53–61.

[4]Robins, R. E., Delisi, D. P., and Greene, G. C., "Development and Validation of a Wake Vortex Predictor Algorithm," AIAA Paper 98-0665, Jan. 1998.

[5]Campbell, S., Dasey, T., Freehart, R., Heinrichs, R., Matthews, M., and Perras, G., "Wake Vortex Field Measurement Program at Memphis, TN," AIAA Paper 96-0399, Jan. 1996.

[6]Campbell, S. D., Dasey, T. J., Freehart, R. E., Heinrichs, R. M., Matthews, M. P., Perras, G. H., and Rowe, G. S., "Wake Vortex Field Measurement Program at Memphis, TN, Data Guide," Lincoln Lab., Massachusetts Inst. of Technology, Project Rept. NASA/L-2, Cambridge, MA, 14 Jan. 1997.

[7]Dasey, T. J., Cole, R. E., Heinrichs, R. M., Matthews, M. P., and Perras, G. H., "Aircraft Vortex Spacing System (AVOSS) Initial 1997 System Deployment at Dallas/Ft. Worth (DFW) Airport," Lincoln Lab., Massachusetts Inst. of Technology, Project Rept. NASA/L-3, Cambridge, MA, 8 July 1998.

[8]Greene, G. C., "An Approximate Model of Vortex Decay in the Atmosphere," *Journal of Aircraft*, Vol. 23, No. 7, 1986, pp. 566–573.

[9]Crow, S. C., "Stability Theory for a Pair of Trailing Vortices," *AIAA Journal*, Vol. 8, No. 12, 1970, pp. 2172–2179.

[10]Robins, R. E., and Delisi, D. P., "Further Development of a Wake Vortex Prediction Algorithm and Comparison to Data," AIAA Paper 99-0757, Jan. 1999.

[11]Sarpkaya, T., "Decay of Wake Vortices of Large Aircraft," *AIAA Journal*, Vol. 36, No. 9, 1998, pp. 1671–1679; see also NASA/CP-97-206235, edited by L. Credeur and R. B. Perry, May 1997, pp. 61–74.

[12]Crow, S. C., and Bate, E. R., "Lifespan of Trailing Vortices in a Turbulent Atmosphere," *Journal of Aircraft*, Vol. 13, No. 7, 1976, pp. 476–482.

[13]Tombach, I., "Observations of Atmospheric Effects on Vortex Wake Behavior," *Journal of Aircraft*, Vol. 10, No. 11, 1973, pp. 641–647.

[14]Sarpkaya, T., and Daly, J. J., "Effect of Ambient Turbulence on Trailing Vortices," *Journal of Aircraft*, Vol. 26, No. 6, 1987, pp. 399–404.

[15]Han, J., Lin, Y.-L., Schowalter, D. G., Arya, S. P., and Proctor, F. H., "Large-Eddy Simulation of Aircraft Wake Vortices Atmospheric Turbulence Effects," *12th Symposium on Boundary Layers and Turbulence*, Univ. of British Columbia, Vancouver, Canada, 1997, pp. 237, 238.

[16]Proctor, F. H., and Switzer, G. F., "Numerical Simulation of Aircraft Trailing Vortices," *9th Conference on Aviation, Range and Aerospace Meteorology*, American Meteorological Society, New York, 2000, pp. 511–516.

[17]Sarpkaya, T., "Trailing Vortices in Homogeneous and Density Stratified Media," *Journal of Fluid Mechanics*, Vol. 136, Nov. 1983, pp. 85–109.

[18]Crow, S. C., and Murman, E. M., "Trailing-Vortex Experiments at Moses Lake," Boeing Scientific Research Lab., communication 009, Seattle, WA, Feb. 1970.

[19]Zheng, Z. C., and Ash, R. L., "Study of Aircraft Wake Vortex Behavior near the Ground," *AIAA Journal*, Vol. 34, No. 3, 1996, pp. 580–589.

[20]Burham, D. C., "B-747 Vortex Alleviation Flight Tests: Ground-Based Sensor Measurements," U.S. Dept. of Transportation, FAA Rept. DOT-TSC-FAA-81-19, Washington, DC, Feb. 1982.

[21]Kantha, L. H., "Empirical Model of Transport and Decay of Wake Vortices Between Parallel Runways," *Journal of Aircraft*, Vol. 33, No. 4, 1996, pp. 752–760.

[22]Kantha, L. H., "Empirical Model of Transport and Decay of Wake Vortices," *Journal of Aircraft*, Vol. 35, No. 4, 1998, pp. 649–653.

[23]Puel, F., and de Saint Victor, X., "Interaction of Wake Vortices with the Ground," *Aerospace Science and Technology*, Vol. 4, No. 4, 2000, pp. 239–247.

[24]Corjon, A., Zheng, Z. C., and Greene, G. C., "Model of the Behavior of Aircraft Wake Vortices Experiencing Crosswind Near the Ground," AIAA Paper 96-2516, Jan. 1996.

[25]Han, J., Shen, S., Arya, S. P., and Lin, Y.-L., "An Estimation of Turbulent Kinetic Energy and Energy Dissipation Rate Based on Atmospheric Boundary Layer Similarity Theory," NASA CR-2000-210298, Aug. 2000.